

Coherent Excitation of Rydberg Atoms in Thermal Vapor Microcells

H. Kübler,¹ J. P. Shaffer,^{1,2} T. Baluktsian,¹ R. Löw,¹ and T. Pfau¹

¹*Physikalisches Institut, Universität Stuttgart, Pfaffenwaldring 57, 70550 Stuttgart*

²*Homer L. Dodge Department of Physics and Astronomy,
The University of Oklahoma, 440 W. Brooks St., Norman, OK 73019*

(Dated: February 3, 2022)

The coherent control of mesoscopic ensembles of atoms and Rydberg atom blockade are the basis for proposed quantum devices such as integrable gates and single photon sources. So far, experimental progress has been limited to complex experimental setups that use ultracold atoms. Here, we show that coherence times of ~ 100 ns are achievable with coherent Rydberg atom spectroscopy in μm sized thermal vapor cells. We investigated states with principle quantum numbers between 30 and 50. Our results demonstrate that microcells with a size on the order of the blockade radius, $\sim 2 \mu\text{m}$, at temperatures of $100 - 300^\circ\text{C}$ are robust, promising candidates to investigate low dimensional strongly interacting Rydberg gases, construct quantum gates and build single photon sources.

Recently, the mutual interaction between highly excited Rydberg atoms in dense frozen samples has lead to the observation of Rydberg atom excitation blockade [1, 2, 3]. In Rydberg atom blockade, the excitation of more than one Rydberg atom within a blockade volume is suppressed as the mutual interaction between Rydberg atoms at internuclear separations on the order of micrometers shifts the atomic state out of resonance with a narrow band excitation laser. The corresponding blockade radius, a_{block} , is on the order of several μm for Rydberg states in the range of $n = 30 - 50$. For example, the 32S state of Rb excited by a 1 MHz bandwidth laser has $a_{\text{block}} = 2 \mu\text{m}$ for an ensemble of atoms that do not move on the timescale of excitation [4]. As the huge interaction between individual Rydberg atoms can lead to controlled entanglement of atomic ensembles, Rydberg atom blockade is the basis for several proposals to realize photonic quantum devices, like single photon sources and quantum gates [5, 6]. The first promising experimental steps toward this goal using individual well localized pairs of ultracold atoms have been reported [7, 8]. Experiments on collective entanglement of ensembles of ultracold atoms have also been performed [1].

A technologically interesting alternative approach to ultracold atoms would be to realize Rydberg atom quantum photonic devices in thermal Rb vapor microcells. For this idea, we envision arrays of small blockade sized vapor cells (cavities) etched in glass that can be connected by optical wave guides in a monolithic structure. In such a device, Rydberg atom quantum gates may be realized with mesoscopic ensembles of thermal atoms. Some of the advantages of this approach are the ability to exploit advances in microstructuring technology [9, 10, 11], the relative simplicity of maintaining and regenerating the sample, the collective enhancement of the laser matter dynamics, and the scalability. We also point out here that a_{block} has a strong scaling with the atomic separation R , proportional to R^6 in the case of Van der Waals interactions. This means that its value for atoms

frozen in place only decreases by approximately 2.7 for a thermal distribution of atoms at $T = 300^\circ\text{C}$, since $a_{\text{block}} \propto \sqrt[6]{\text{Doppler width}}$.

An important point for using mesoscopic ensembles of atoms confined to a blockade volume is that they can be used to realize so called "superatoms", where collective ground and excited states mimic the behavior of an individual atom with coherent collectively enhanced dynamics [1, 12]. The collective behavior allows for fast manipulations of the qubits and provides immunity to noise and processing errors [5]. The requirements for collective quantum dynamics in a mesoscopic ensemble of Rydberg atoms are a density of ground state atoms much larger than $(a_{\text{block}})^{-3}$ and a timescale for the coherent dynamics that is short compared to the time the atoms need to move one excitation wavelength. The first requirement guarantees a substantial enhancement of the collective dynamics. The second requirement is necessary to assure that the dynamics of the ensemble are collective and coherent. Thermal Rb vapors spatially confined to $\sim \mu\text{m}$ length scales can provide the required densities at temperatures around $100 - 300^\circ\text{C}$. Due to their thermal velocities coherent collective dynamics are expected to be limited to a timescale of a few nanoseconds. The timescale requirement can be met in a thermal vapor cell by using nanosecond pulsed bandwidth limited laser excitation [13] provided there are no further dephasing or decoherence mechanisms active on that timescale or shorter [11, 14]. Under similar conditions, strongly interacting, low dimensional, Rydberg gases can be investigated. In this case, low dimensional means that some or all of the geometric dimensions of a structure are on the order of or less than a_{block} .

The very quality that Rydberg atoms possess which is the fundamental root of the dipole blockade effect, namely a large polarizability, also leads to their strong interaction with nearby walls and electric fields. While the Casimir Polder effect between Rydberg atoms and a metallic surface has been investigated [15], the effect of

dielectric walls on Rydberg atoms is virtually unknown. The effect of dielectric surfaces on Rydberg atoms are expected to be stronger than a metal surface because a dielectric surface can become charged and the surface interaction can be enhanced by the resonant interaction with surface polaritons [15, 16, 17, 18]. The effect of the microcell's walls can be a serious impediment to implementing them to make quantum photonic devices.

In this paper we study coherent Rydberg excitation of a thermal vapor in a confined geometry, a two dimensional microcell, using Rydberg state electromagnetically induced transparency (EIT) [19]. The technique probes the Rydberg state energy shifts and line broadening. We observe an EIT signal at $\sim 1 \mu\text{m}$ separation between two confining dielectric quartz walls for some states in the range $n=30-50$, contrary to common expectations of very broad and massively shifted Rydberg spectra [15]. In particular, for 32S we observe linewidths on the order of $\sim 12 - 16 \text{ MHz}$. This fact indicates that coherent collective dynamics in a thermal microcell are not fundamentally limited by wall induced decoherence or dephasing effects provided the correct Rydberg state is chosen. The corresponding coherence times also demonstrate that Rb vapor microcells can be good candidates for realizing scalable arrays of quantum gates. This is a significant step toward realizing an entirely new system that can be used for quantum photonic devices, such as single photon sources, quantum memories, and gates all based on the same technology.

ELECTROMAGNETICALLY INDUCED TRANSPARENCY IN MICROCELLS

In all experiments described below, a wedge shaped vapor cell with a Rb reservoir attached to it is used. The slope of the wedged gap was interferometrically found with a Michelson interferometer to be $10.5 \mu\text{m mm}^{-1}$ and also indicated that the flats were in contact at the narrow gapped edge of the cell. To make sure that the flats are contacting each other, Newton rings were observed in the thin region of the wedge. The maximum gap thickness was $500 \mu\text{m}$.

The wedged part of the cell and the reservoir are placed in separate ovens, Fig. 1. This way the temperature of the wedge and reservoir can be varied independently. The wedge is kept at higher temperatures than the reservoir to prevent condensation of Rb on its surface. By changing the temperatures of the two ovens, the Rb vapor pressure and therefore the Rb density can be controlled. The Rb vapor density used for the experiments was $1.6 \times 10^{14} \text{ cm}^{-3}$. This corresponds to a Rb vapor pressure of 4.4 mTorr in the microcell, which dominates all others.

EIT is chosen as the method to probe the behavior of the Rydberg atoms in the cell because, as a coherent

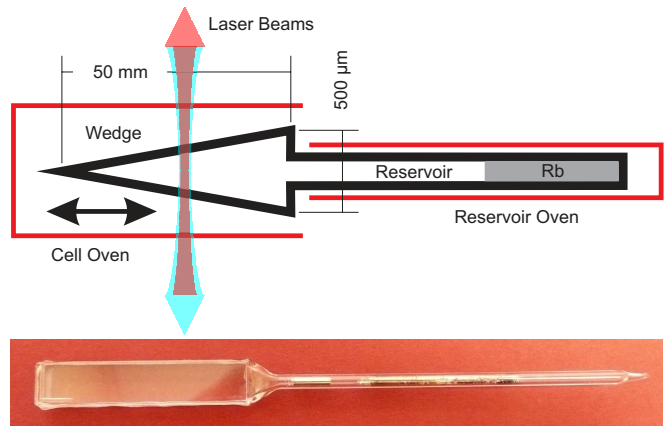


FIG. 1: Experimental setup. Two ovens allow for the control of the temperature of the wedge and reservoir so that the Rb density can be set. Moving the cell relative to the laser beams changes the thickness of the Rb vapor layer. An image of the cell is shown.

type of spectroscopy, it is a direct measurement of the dephasing mechanisms of the Rydberg state and of the Rydberg state energy shift. Since EIT depends on quantum interference between the probe transition and probe plus coupling laser transition, EIT is exquisitely sensitive to phase disturbances on the coupling laser transition. Energy level shifts of the Rydberg state cause the transmission window of the probe laser to shift in frequency as well. To study the Rydberg states we use EIT in a ladder configuration. We use a counterpropagating laser geometry. The states involved in the EIT scheme used for this work for a given Rydberg state, nl , are $5S_{1/2} \rightarrow 5P_{3/2} \rightarrow nl$, Fig. 2. The first transition, called the probe transition, occurs at $\sim 780 \text{ nm}$ while the Rydberg transition, called the coupling transition, is at $\sim 480 \text{ nm}$. Principle quantum numbers between 30 and 50 of ^{87}Rb have been investigated both for $l = 0$ and $l = 2$.

The peak Rabi frequency of the probe laser transitions is 5 MHz and the peak Rabi frequency of the coupling laser transition is 9 MHz for 32S . The intensity of the coupling laser was adjusted to maintain these Rabi frequencies for the other Rydberg states that were studied. Signal detection in the narrow part of the cell prevented us from decreasing the Rabi frequencies further. Under these conditions, the total fraction of atoms in the Rydberg state is $\sim 3 \times 10^{-5}$, yielding a Rydberg atom density of $\sim 5 \times 10^9 \text{ cm}^{-3}$ for 32S . The density is chosen so that Rydberg-Rydberg interactions are negligible. For $32\text{S}+32\text{S}$, the expected Van der Waals interaction is less than $\sim 1 \text{ MHz}$.

The probe laser light that is transmitted through the cell is coupled to a single mode fiber and measured by a photo multiplier tube. The probe laser is locked to the $5S_{1/2}(F = 2) \rightarrow 5P_{3/2}(F = 3)$ transition. The coupling

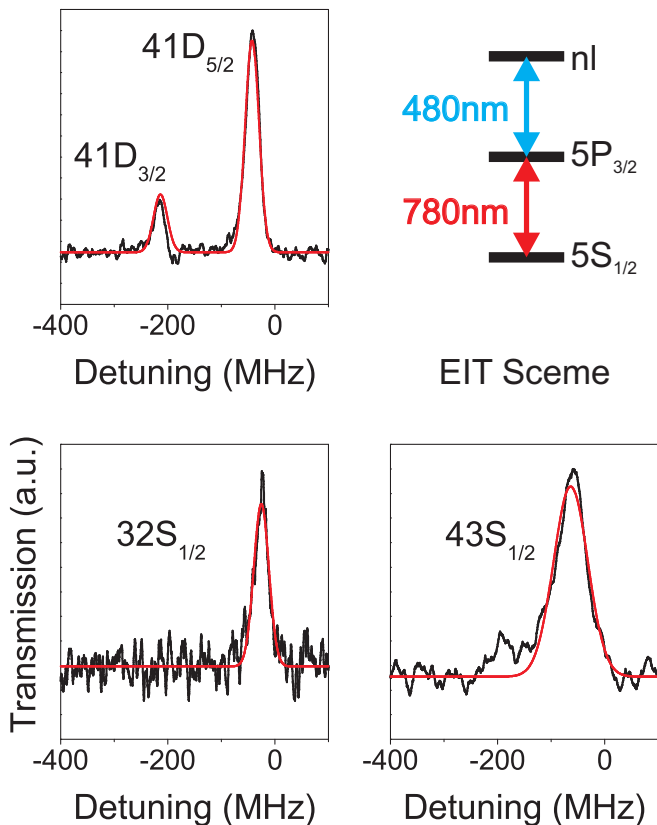


FIG. 2: EIT scheme and transmission signals as a function of frequency. The 43S and 41D data were taken at wedge thicknesses of $100\text{ }\mu\text{m}$. The 32S data was taken at a wedge thickness of $60\text{ }\mu\text{m}$. The other experimental parameters are described in the text. The lines are fits of the data to a Gaussian lineshape. The EIT level scheme is also shown.

laser light is intensity modulated using an acousto-optic modulator (AOM) at a frequency of 100 kHz . The change in probe transmission correlated to the presence of the coupling laser is measured with a lock-in amplifier as a function of coupling laser frequency. The coupling laser frequency is scanned at a rate of $\sim 400\text{ MHz s}^{-1}$. Up to 12,000 transmission curves are averaged per data point to obtain the EIT signal. The probe and coupling laser frequencies are referenced to an EIT signal that is obtained with a 10 cm long Rb vapor cell in co- and counter propagating laser geometry. We estimate the frequency stability of the EIT signal at $\sim 2\text{ MHz}$ over the course of averaging $\sim 12,000$ transmission curves.

RESULTS AND DISCUSSION

First, we used a gap size large enough so that wall interactions were negligible. Fig. 2 shows the 43S and the 41D EIT signals in a $100\text{ }\mu\text{m}$ and the 32S EIT signal in a $60\text{ }\mu\text{m}$ thick section of the wedge. The fine structure of the 41D state is clearly visible. For these

states, wedge thicknesses and experimental conditions already described, the transmission signal has a linewidth of $\sim 12 - 16\text{ MHz}$. The linewidth in this part of the cell is determined by line broadening due to ground state Rb atoms colliding with atoms in their Rydberg states [20], laser frequency stability, transit time broadening, and power broadening. In these regions of the cell, the quartz walls have little effect on the EIT lineshape.

If we assume a thermal velocity of $v \approx 366\text{ m s}^{-1}$, consistent with the cell temperature of 195°C , the laser spot size leads to a transit time broadening of $\sim 4\text{ MHz}$. Collision broadening is dominated by collisions between ground state atoms and Rydberg atoms. Collisions involving only ground state and $5P_{3/2}$ atoms have much smaller cross-sections while collisions between $5P_{3/2}$ atoms and Rydberg atoms are much less frequent because the density of $5P_{3/2}$ and Rydberg atoms is much less than the ground state atoms. The collisional broadening due to ground state atoms colliding with the Rydberg atoms has been measured for Rb [20]. For our temperatures and densities, kept constant for these experiments, the collision broadening is $\sim 11\text{ MHz}$. Taking into account the Rabi frequencies, laser stability over the time of the measurement, transit time broadening and collisional broadening, we estimate a minimum width of the EIT transmission signal of $\sim 14\text{ MHz}$, in excellent agreement with the measurements taken in parts of the wedge where the wall interactions are negligible. Errors in the measured linewidth are most likely due to differences in laser drift and Rb gas density fluctuations during different data runs.

We have taken special care in determining the electric fields that can lead to both line shifts and broadening. Charges can buildup on the walls of the cell because it is a dielectric. The electric field created by these charges can cause the Rydberg state to shift in energy. If the distribution of charges is not uniform, then the electric field will be inhomogeneous and will also cause a broadening of the EIT signal. We made several measurements of the electric field to verify that it did not dominate the Casimir-Polder forces in the smaller sections of the wedge and that the inhomogeneous electric fields can be overcome in order to use microcells for quantum photonic devices. From these measurements, we conservatively estimate the electric field at $< 4\text{ V cm}^{-1}$ in the $\sim 1\text{ }\mu\text{m}$ part of the cell. The electric field inhomogeneities were not detectable in the experiments. The estimates of the electric field in the microcell also suggest that field ionization of the Rydberg atom is not an issue even in the $\sim 1\text{ }\mu\text{m}$ parts of the wedge. Magnetic field effects are not important in the work here and can be safely neglected.

In the thinner regions of the wedge, $< 20\text{ }\mu\text{m}$, the wall interactions dominate the dephasing and also shift the Rydberg state energy. There are two components to the forces that the Rydberg atoms experience due to the presence of the wall [16, 17]. First, there is the interaction

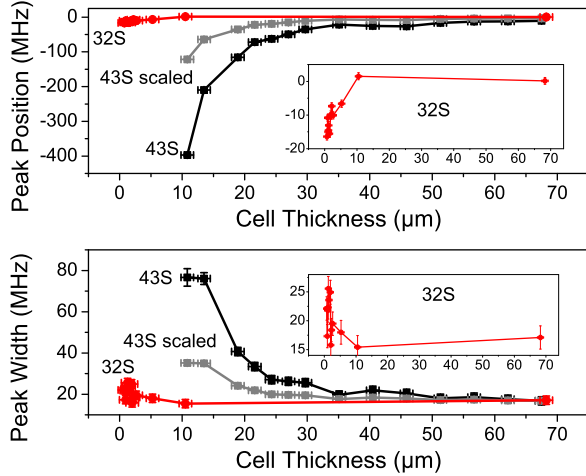


FIG. 3: A comparison of the shift and broadening as a function of wedge thickness for the 32S and 43S states. The curve labeled 43S scaled is the data for the 43S state scaled to the dipole moment of the 32S state. This curve shows that the weaker 32S interaction with the cell wall is not due only to the differences in the dipole moments. The scaling is described in more detail in the text. The horizontal error bars show the uncertainty in the wedge thickness. The vertical error bars show the fitting error and the point to point variation as determined by variation in the measurements at wedge thickness $> 50 \mu\text{m}$.

of the atom with its image. This interaction essentially takes into account the boundary conditions on the electromagnetic field due to the quartz wall. It is $\sim 8 \text{ MHz}$ for 43S and $\sim 2 \text{ MHz}$ for 32S at $R = 2 \mu\text{m}$ [16, 21], where R is the distance between the wall and atom. Secondly, the Rydberg atom can couple resonantly to the surface polariton modes of the quartz. As this interaction depends on the microscopic properties of the quartz, a detailed estimate of its size is beyond the scope of this paper and will be the subject of an additional work in the near future. The interaction with surface polariton modes can be large for Rydberg atoms because the energy intervals between dipole coupled Rydberg states can match those of far infrared active polariton modes. It is therefore important to choose a Rydberg state and microcell material so that the resonant couplings between the Rydberg state and polariton modes, including those from thermally excited polaritons, are minimized in order to maximize the coherence time of the atoms in a microcell. In our experiment, minimization of the overlap between the resonances of the dielectric and the Rydberg atoms is the essential point that allows for coherence times of roughly 100 ns even at a cell thickness of $\sim 1 \mu\text{m}$.

The 43S state data exhibits strong effects from its interaction with the quartz walls, as shown in Fig. 3. At a cell temperature of 195°C and a reservoir temperature of

150°C we observed line broadenings up to 75 MHz and a shift of 400 MHz at a cell thickness of $10 \mu\text{m}$. We attribute this behavior to a strong interaction with surface polaritons. Note that some surface polariton modes are thermally excited at 195°C . These modes can lead to other second order energy exchange pathways between Rydberg states where one polariton can be annihilated and another one can be created. These thermally activated pathways are enabled by transitions with smaller differences in principle quantum number and therefore possess larger dipole transition matrix elements.

A spectrum as a function of wedge thickness for the 32S state is shown in Fig. 4. In contrast to the 43S data, we observed narrow and only marginally shifted EIT lines all the way down to $\sim 1.0 \mu\text{m}$, Fig. 3. The linewidths were 12 – 16 MHz and the maximum shift was 16 MHz at a cell temperature of 195°C . The reservoir was kept at 150°C . These conditions are the same as for the 43S measurement. 32S has the smallest coupling to the walls that we have observed so far. We attribute this result to the fact that the 32S state has the fewest overlaps between its allowed dipole transitions and infrared active transitions between polariton states. The differences between the 32S and the 43S states cannot be explained by the scaling of the respective dipole moments. A plot of the 43S data scaled according to the n^4 dependence [16] of the interaction due to the different dipole moments is shown in Fig. 3. The magnitude of the shift of the 32S state is approximately what is expected from the interaction of the atom with its image in the dielectric taking into account the dominant transition to the nearest P states [16, 21].

The 41D state shows additional evidence for the presence of resonant wall interactions, Fig. 5. The interaction of the atom with its image does not depend on polarization [15, 16, 17]. The resonant interaction that involves atoms interacting with the surface polaritons is polarization dependent because of the dipole selection rules that govern the allowed transitions for energy exchange with the wall. For the 41D state we have observed a gap and temperature dependent splitting of the m_J sub-levels of each of its fine structure components, Fig. 5. We observe one group of states that is shifted and broadened similar to the 43S state, whereas other states at the same time are not affected. This cannot be explained by a Boltzmann factor weighting of the dominant dipole transition. The temperature dependence of the dominant dipole transition is very weak over the small range of temperatures we investigated, 100 – 300°C . The fact that different m_J states have different behavior supports our statement that the resonant wall interactions are important since this has to result from a polarization dependent interaction. Similar observations were obtained for the 30D state.

Further systematic investigations of the details of the atom wall coupling are clearly necessary and are the sub-

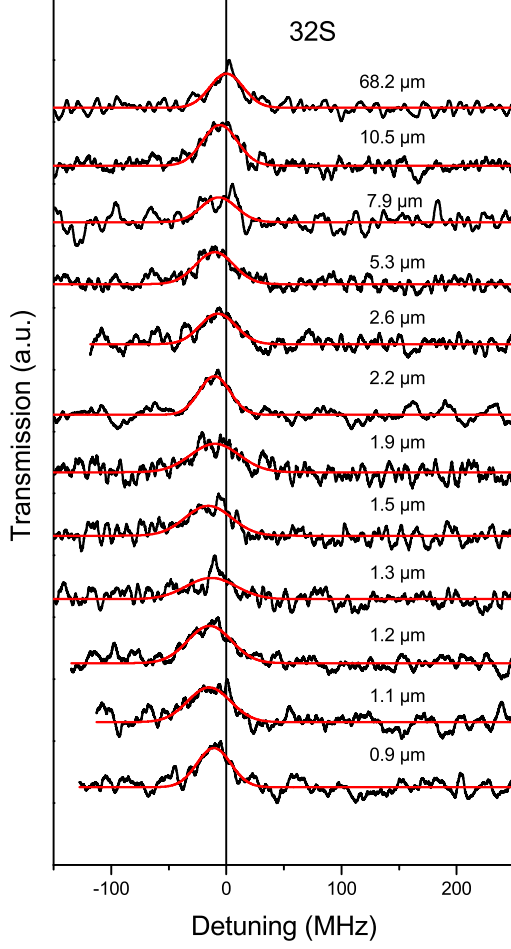


FIG. 4: The transmission curves of the 32S state as a function of frequency and thickness. The experimental parameters are described in the text of the paper. The lines show Gaussian fits to the data. The vertical line shows the zero of frequency as determined from the reference signal obtained from the 10 cm Rb cell. The uncertainty in the wedge thickness is $\sim \pm 1 \mu\text{m}$.

ject of further studies. However, the fact that it is possible to observe Rydberg atoms with linewidths and shifts on the 10 MHz level is very encouraging for further investigations toward collective coherent quantum dynamics in microcells. The data leads us to the conclusion that the overlap between the polariton resonances of the walls and the Rydberg atoms have to be reduced to obtain a coherence time such that it is possible to realize Rydberg atom blockade in a microcell.

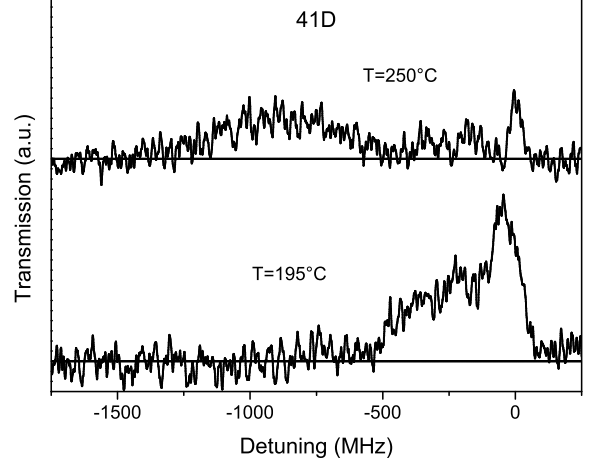


FIG. 5: 41D state. This plot shows the 41D state at two different temperatures at a wedge thickness of $80 \mu\text{m}$.

CONCLUSION

To summarize, we have measured the dephasing and energy level shifts experienced by Rydberg states in microcells with thicknesses on the order of a_{block} using EIT. For 43S we observed a significant wall induced line shift and broadening. The magnitude of these effects in the $\sim \mu\text{m}$ region of the cell prevented us from obtaining a suitable signal for coherent spectroscopy. For the 41D state we observed a group of states strongly coupled to the surface and another one that remained narrow - evidence for a dark state with respect to the atom wall coupling. We obtained our best results for the 32S state. This state does not have resonant overlap with the known polariton lines of quartz [22] and we observe an EIT signal that is suitable for coherent manipulations of the dynamics in the $\sim 1 \mu\text{m}$ region of the cell. The frequency shifts and line broadening are only on the order of a few 10 MHz. This is significantly less than the bandwidth required for collective coherent dynamics in a thermal vapor cell as discussed in the introduction of this paper. Therefore we expect that collective coherent dynamics are possible in a thermal microcell.

Our measurement is encouraging for further investigations that are necessary for realizing single photon sources and other quantum devices based on Rydberg atom blockade in thermal microcells. The significant achievement of this study is the demonstration that there are Rydberg states that can have long enough coherence times to take advantage of the dipole blockade effect in thermal microcells. In contrast to collective dynamics involving electronic transitions, for example Rydberg states, the collective dynamics of nuclear spin states are expected to have a significantly longer coherence time,

especially if spin protective coatings or buffer gas loaded cells are used. Future studies will utilize cells that make use of conductive coatings to eliminate residual electric field effects and ones coated and filled with buffer gas to enhance the coherence times of nuclear spin states. Optimized cell materials and surface structures can also be used to minimize the interactions of polaritons and Rydberg atoms.

METHODS

The cell was fabricated from two quartz optical flats (Herasil 1) of thickness of 5 mm, cut to a size of $5\text{ cm} \times 1\text{ cm}$. To form the cell, a spacer of $500\text{ }\mu\text{m}$ thickness is placed between the flats to make a 5 cm long wedge with a maximum gap of $500\text{ }\mu\text{m}$. All the edges of the wedge, except the one where the spacer is placed, are sealed by fusing the glass. Next, the spacer is removed and a tube is connected to the open side of the wedge and the wedge is sealed. The cell is pumped through the tube to pressures below 10^{-6} mbar, the tube is partially filled with Rb and is finally sealed off. The tube acts as the reservoir.

The oven used to heat the wedge has 2 windows so that the light used for the experiment can pass through the cell. This oven heats the wedge uniformly without obstructing optical access. The Rb density is monitored by absorption measurements on the $\text{Rb } 5\text{S}_{1/2} \rightarrow 5\text{P}_{3/2}$ transition. From fits of the absorption spectra we were able to reproduce the wedge temperature to within $\pm 5^\circ\text{C}$. Therefore, we were able to control the Rb density and optical density in the wedged cell.

The coupling and probe beams pass through the oven windows, optical flats and vapor in a counter propagating geometry, essentially normal to the surface of the cell, Fig. 1. The position of the beams along the wedge can be changed by moving the cell in and out of the oven heating the wedge on a translation stage. This allows the thickness of the gap and consequently the Rb vapor to be set for a given experiment. The accuracy of the cell thickness is better than $1\text{ }\mu\text{m}$.

The probe laser has a power of $16\text{ }\mu\text{W}$ and is focussed to a beam waist of $237\text{ }\mu\text{m}$. The coupling laser has a power of $800\text{ }\mu\text{W}$ for 32S and is focussed to a beam waist of $193\text{ }\mu\text{m}$. The laser-matter interaction region is cylindrical with a diameter of $193\text{ }\mu\text{m}$ and length equal to the size of the wedge gap. The Rayleigh ranges of the focussed beams are much longer than the cell gap width for all the data presented here. The coupling laser has a bandwidth of 2 MHz over a ms timescale. The probe laser bandwidth is approximately the same. The coupling laser bandwidth is more important because the Rydberg linewidth is narrow compared to the laser bandwidth, thus reducing the effective Rabi frequency delivered on the coupling transition.

The reference cell is a 10 cm long Rb vapor cell in co-

and counter propagating laser geometry. To determine the reference signal, a fraction of the probe laser is shifted with an AOM 200 MHz to supply the probe light for the reference cell. The coupling laser light used in the reference cell is derived from the same source as that in the thin cell. This light is frequency shifted 200 MHz and amplitude modulated at 100 kHz with a π phase shift relative to that used for experiments in the thin cell. A second lock-in amplifier is used for this setup. The co- and counter-propagating EIT signals provide a well defined calibration of the frequency via the differential Doppler effect. Additionally, each scan is triggered on the counter-propagating signal to provide a stable locking point for the averaging of the scans.

The Stark shifts for alkali-atom Rydberg states are well known and there are highly accurate methods to compute them [23]. Consequently, the field inside the cell can be estimated by measuring the line splitting of a D state or the shift of an S state. We observed a wall distance dependent line splitting for the 41D state from which we determined the electric field to be $< 3.6\text{ Vcm}^{-1}$ at $\sim 1\text{ }\mu\text{m}$ wedge gap. The measured electric field depended linearly on the wedge gap which is evidence that the charges were on the surfaces of the wedge. This measurement was done in the larger, $> 20\text{ }\mu\text{m}$, sections of the wedge to avoid mixing the Stark shift caused by the surface charges with the interaction between the dielectric wall and the Rydberg atoms. In addition, for the 32S state, which was observed to have a weak interaction with the walls, we observed only a small shift. This data places an upper limit on the electric field in the $\sim 1\text{ }\mu\text{m}$ part of the wedge at $\sim 4\text{ Vcm}^{-1}$, consistent with the electric field measurement performed using the 41D state splittings. This estimate is an upper limit since it attributes all the observed shift to an electric field. A third piece of data that supports our field measurements is the fact that we do not observe the blue shift of the $m_J = 1/2$ 41D_{5/2} or the $m_J = 1/2$ 41D_{3/2} states. From the 41D Stark map this observation indicates that the field is smaller than 1.2 Vcm^{-1} at a gap of $20\text{ }\mu\text{m}$ and suggests that the other measurements are upper bounds and in fact the electric field may be smaller.

ACKNOWLEDGMENTS

We acknowledge fruitful discussions with H.P. Büchler and H. Giessen as well as financial support from the Landesstiftung Baden-Württemberg. J. P. Shaffer acknowledges support by the Alexander von Humboldt Foundation.

AUTHOR CONTRIBUTIONS

All authors contributed extensively to the work presented in this paper.

REFERENCES

-
- [1] Heidemann, R., Raitzsch, U., Bendowsky, V., Butscher, B., Löw, R., Santos, L. and Pfau, T. Evidence for Coherent Collective Rydberg Excitation in the Strong Blockade Regime. *Phys. Rev. Lett.* **99**, 163601/1-163601/4 (2007).
 - [2] Tong, D., Farooqi, S.M., Stanojevic, J., Krishnan, S., Zhang, Y.P., Coté, R., Eyler, E.E. and Gould, P.L. Local Blockade of Rydberg Excitations in an Ultracold Gas. *Phys. Rev. Lett.* **93**, 63001/1-63001/4 (2004).
 - [3] Singer, K., Reetz-Lamour, M., Amthor, T., Marcassa, L.G. and Weidemüller, M. Suppression of Excitation and Spectral Broadening Induced by Interactions in a Cold Gas of Rydberg Atoms. *Phys. Rev. Lett.* **93**, 163001/1-163001/4 (2004).
 - [4] Schwettmann, A., Crawford, J., Overstreet, K.R., and Shaffer, J.P. Cold Cs Rydberg-gas interactions. *Phys. Rev. A* **74**, 020701(R)/1-020701(R)/4 (2006).
 - [5] Saffman, M. and Mølmer, K. Efficient Multiparticle Entanglement via Asymmetric Rydberg Blockade. *Phys. Rev. Lett.* **102**, 240502/1-240502/4 (2009).
 - [6] Lukin, M.D., Fleischhauer, M., Coté, R., Duan, L.M., Jaksch, D., Cirac, J.I. and Zoller, P. Dipole Blockade and Quantum Information Processing in Mesoscopic Atomic Ensembles. *Phys. Rev. Lett.* **87**, 37901/1-37901/4 (2001).
 - [7] Urban, E., Johnson, T.A., Henage, T., Isenhower, L., Yavuz, D.D., Walker, T.G., Saffman, M. Observation of Rydberg Blockade Between Two Atoms. *Nature Phys.* **5**, 110-114 (2009).
 - [8] Gaetan, A., Miroshnychenko, Y., Wilk, T., Chotia, A., Viteau, M., Comparat, D., Pillet, P., Browaeys, A., and Grangier, P. Observation of Collective Excitation of Two Individual Atoms in the Rydberg Blockade Regime. *Nature Phys.* **5**, 115-118 (2009).
 - [9] Sharping, J.E. Rubidium on a Chip. *Nature Phot.* **1**, 315-316 (2007).
 - [10] Yang, W., Conkey, D.B., Wu, B., Yin, D., Hawkins, A.R., and Schmidt, H. Atomic Spectroscopy on a Chip. *Nature Phot.* **1**, 331-335 (2007).
 - [11] Löw, R. and Pfau, T. Magneto-Optics: Hot Atoms Rotate Light Rapidly. *Nature Phot.* **3**, 197-199 (2009).
 - [12] Duan, L.-M., Lukin, M.D., Cirac, J.I., and Zoller, P. Long-Distance Quantum Communication with Atomic Ensembles and Linear Optics. *Nature* **414**, 413-418 (2001).
 - [13] Schwettmann, A., McGuffy, C., Chauhan, S., Overstreet, K.R. and Shaffer, J.P. A Tunable Four Pass Narrow Spectral Bandwidth Amplifier for Use at 500nm. *Applied Optics* **46**, 1310-1315 (2007).
 - [14] Siddons, P., Bell, N.C., Cai, Y., Adams, C.S. and Hughes, I.G. A gigahertz-bandwidth atomic probe based on the slow-light Faraday effect. *Nature Phot.* **3**, 225-229 (2009).
 - [15] Hinds, E.A., Lai, K.S., and Schnell, M. Atoms in Micron-Sized Metallic and Dielectric Waveguides. *Phil. Trans. R. Soc. Lon. A* **355**, 2353-2365 (1997).
 - [16] Barton, G. Van der Waals Shifts in an Atom Near Absorptive Dielectric Mirrors. *Proc. R. Soc. Lon. A* **453**, 2461-2495 (1997).
 - [17] Wylie, J.M. and Sipe, J.E. Quantum Electrodynamics Near an Interface. *Phys. Rev. A* **32**, 2030-2043 (1985).
 - [18] Failache, H., Saltiel, S., Fichet, M., Bloch, D., and Ducloy, M. Resonant Coupling in the Van der Waals Interaction Between an Excited Alkali Atom and a Dielectric Surface: An Experimental Study via Stepwise Selective Reflection Spectroscopy. *Eur. Phys. J. D* **23**, 237-255 (2003).
 - [19] Mohapatra, A.K., Jackson, T.R., and Adams, C.S. Coherent Optical Detection of Highly Excited Rydberg States Using Electromagnetically Induced Transparency. *Phys. Rev. Lett.* **98**, 113003/1-113003/4 (2007).
 - [20] Thompson, D.C., Weinberger, W., Xu, G.-X., and Stoiceff, B.P. Frequency Shifts and Line Broadenings in Collisions Between Rydberg Atoms and Ground-State Alkali-Metal Atoms. *Phys. Rev. A* **35**, 690-700 (1987).
 - [21] Hoogenraad, J.H. and Noordam, L.D. Rydberg Atoms in Far-Infrared Radiation Fields. I. Dipole Matrix Elements of H, Li, and Rb. *Phys. Rev. A* **57**, 4533-4545 (1998).
 - [22] Spitzer, W.G. and Kleinman, D.A. Infrared Lattice Bands of Quartz. *Phys. Rev.* **121**, 1324-1334 (1961).
 - [23] Zimmerman, M.L., Littman, M.G., Kash, M.M., and Kleppner, D. Stark Structure of the Rydberg States of Alkali-Metal Atoms. *Phys. Rev. A* **20**, 2251-2275 (1979).